Provenance of Ordovician–Silurian and Carboniferous–Permian glaciogenic successions in Ethiopia revealed by detrital zircon U–Pb geochronology

Abbreviated title: Zircon chronology Palaeozoic Ethiopia

Anna Lewin[1]*, Guido Meinhold[2,3], Matthias Hinderer[1], Enkurie L. Dawit[4], Robert Bussert[5] & Jasper Berndt[6]

[1] Institute of Applied Geosciences, Darmstadt Technical University, Schnittspahnstraße 9, 64287 Darmstadt, Germany

[2] School of Geography, Geology and the Environment, Keele University, Keele, Staffordshire, ST5 5BG, United Kingdom

[3] Geowissenschaftliches Zentrum Göttingen, Abteilung Sedimentologie / Umweltgeologie, Universität Göttingen, Goldschmidtstraße 3, 37077 Göttingen, Germany

[4] Department of Geology, University of Gondar, P.O. Box 196, Gondar, Ethiopia

[5] Department of Applied Geosciences, Berlin Technical University, Ernst-Reuter-Platz 1, 10587 Berlin, Germany

[6] Institut für Mineralogie, Westfälische Wilhelms-Universität Münster, Corrensstraße 24, 48149 Münster, Germany

*Correspondence: alewin@geo.tu-darmstadt.de

Abstract: Palaeozoic sedimentary successions in northern Ethiopia contain evidence for two Gondwana glaciations during the Late Ordovician and Carboniferous–Permian. We compare sediments of the two glaciations regarding their detrital zircon U–Pb ages. The main age group for both formations is Pan-African (*c*. 550–700 Ma). However, the remaining spectra are different: The Upper Ordovician–Lower Silurian Enticho Sandstone is characterised by a Stenian–Tonian (*c*. 1 Ga) zircon population. The Carboniferous–Permian Edaga Arbi Glacials contain a prominent *c*. 800 Ma population. The Stenian–Tonian zircons are likely derived from the

centre of the East African Orogen and were supplied via the Gondwana super-fan system. This material was transported by the Late Ordovician glaciers and formed the Enticho Sandstone. Tonian (*c.* 800 Ma) zircons are abundant in the Ethiopian basement and represent the earliest formation stage of the southern Arabian–Nubian Shield. Glaciers of the Late Palaeozoic Ice Age must have cut deeply into the basement for efficient erosion. No recycling of the Enticho Sandstone by the Edaga Arbi Glacials took place on a grand scale — probably because sedimentation of the former was limited to northern Ethiopia, whereas the source area for the latter was to the south.

Keywords: Gondwana, Ethiopia, Palaeozoic, glacial sediments, detrital zircon, U–Pb geochronology, Enticho Sandstone, Edaga Arbi Glacials

Supplementary material: A detailed description of the analytical parameters and supplementary data are available at https://doi.org/10.6084/m9.figshare.c.4605548.

The Gondwana supercontinent comprised Archaean to Mesoproterozoic cratons surrounded by Neoproterozoic mobile belts. These belts include juvenile crust and crust that was reactivated in the orogenic processes (e.g. Stern 1994; Burke *et al.* 2003; Collins & Pisarevsky 2005; Fig. 1). The East African Orogen (EAO) that formed between 650 and 600 Ma at the suture of East and West

Gondwana is regarded as one of the largest accretionary orogens in the Earth's history (Stern 1994; Collins & Pisarevsky 2005; Squire *et al*. 2006). In northern Africa, a vast peneplain developed after the consolidation of the newly formed continent, on which a blanket of Palaeozoic sandstone was deposited (Garfunkel 2002; Avigad *et al.* 2005). The sediment transport direction during the early Palaeozoic is generally assumed to the north towards the margin of Gondwana (e.g. Meinhold *et al*. 2011; Morag *et al.* 2011; Avigad *et al.* 2012). The high maturity of the North Gondwana Lower Palaeozoic sandstones is striking. It can be attributed either to long transport distance and/or multiple recycling (e.g. Garfunkel 2002; Morag *et al.* 2011) or strong chemical weathering at the time of deposition (e.g. Avigad *et al.* 2005). Based on the similarity of detrital zircon U–Pb age spectra throughout Gondwana, Squire *et al.* (2006) postulated the existence of large sediment fans that brought detritus from the East African Orogen towards the continental margins. In a compilation of detrital zircon age spectra from Cambrian–Ordovician sandstones of North Africa and NW Arabia Meinhold *et al.* (2013) extended the super-fan model to the northern Gondwana margin. Ethiopia would hence lie more proximal along the sediment path. Here, the Palaeozoic is mainly composed of sedimentary rocks related to the two Gondwana glaciations: 1) the Enticho Sandstone, deposited during the Late Ordovician (Hirnantian) glaciation and the following transgression, probably up to the early Silurian and 2) the Edaga Arbi Glacials that formed during the Carboniferous–Permian glaciation. The Late Ordovician glaciation was short-lived and affected large parts of Gondwana synchronously (e.g. Eyles 1993; Ghienne *et al.* 2007; Le Heron & Craig 2008; Le Heron *et al*. 2018). For the Late

Palaeozoic Ice Age (LPIA) that affected Ethiopia in the Carboniferous–Permian a more complex spatial and temporal pattern of ice sheets is likely (e.g. Eyles 1993; Bussert & Schrank 2007; Fielding *et al.* 2008; Bussert 2014).

In this study, we have analysed 11 sandstone samples of the Upper Ordovician–Lower Silurian Enticho Sandstone and the Carboniferous–Permian Edaga Arbi Glacials for their detrital zircon U–Pb ages to link them to potential source areas. We further aim to:

- Test the Gondwana super-fan hypothesis (Squire *et al.* 2006; Meinhold *et al.* 2013) at a more proximal location,
- Review the assumption of a distant provenance for the Enticho Sandstone and a proximal provenance for the Edaga Arbi Glacials (Lewin *et al.* 2018).

Geological setting

In Ethiopia, outcrops of the Palaeozoic successions are present around the Mekelle Basin in the Tigray province of northern Ethiopia and to a minor extent in the Blue Nile region in the west of the country (Kazmin 1972; Garland 1978; Tsige & Hailu 2007; Fig. 2). Sedimentological and palynological studies on these successions have been carried out by Dow *et al.* (1971), Beyth (1972a, b), Saxena & Assefa (1983), Bussert & Schrank (2007), Bussert & Dawit (2009), Bussert (2014) and Dawit (2014). The two studied formations overlie the Neoproterozoic basement and are overlain by uppermost Palaeozoic and Mesozoic sediments (Beyth 1972b; Tefera *et al.* 1996; Dawit 2010, 2014; Fig. 2).

The basement in Ethiopia represents the junction of the Arabian–Nubian Shield (ANS) in the north and the Mozambique Belt (MB) in the south, together making up the East African Orogen (Kazmin *et al.* 1978; Tefera *et al.* 1996; Stern *et al.* 2012; Fig. 1). The Arabian–Nubian Shield comprises a collage of Neoproterozoic juvenile arcs, younger sedimentary and volcanic basins, voluminous granitoid intrusions and few enclaves of pre-Neoproterozoic crust (Johnson *et al.* 2011). Woldemichael *et al.* (2010) described the evolution of the Arabian–Nubian Shield in a super-continent cycle from the break-up of Rodinia to the amalgamation of Gondwana: early rifting began around 900–860 Ma. With the opening of the Mozambique Ocean, a passive margin formed in the area and early intrusions were emplaced around 860–830 Ma. Subduction and back-arc formation began at 830–750 Ma, followed by terrane accretion, metamorphism, and syn-tectonic intrusions. The ocean closed around 750–650 Ma with further accretion and intrusions. Between 650–550 Ma, the Arabian–Nubian Shield assembly was in its final stage, and metamorphism as well as post-tectonic intrusions occurred. The rocks of the Arabian–Nubian Shield were metamorphosed at low-grade greenschist facies (Beyth 1972b; Alene *et al.* 2006; Stern 2008).

In contrast, the Mozambique Belt to the south comprises medium- to high-grade gneisses and amphibolites as well as granulites. Here, the Ediacaran collision between East and West Gondwana was most intense. Mountains rose to a great height and were eroded in the Late Ediacaran and Early Palaeozoic (Stern *et al.* 2012). The Mozambique Belt contains large amounts of Archaean to Mesoproterozoic crust

that was reworked during Neoproterozoic metamorphism and anatexis; yet subordinate amounts of juvenile Neoproterozoic igneous rocks are present (Stern 2008; Johnson *et al.* 2011; Fritz *et al.* 2013).

The basement of northern Ethiopia is considered part of the Arabian–Nubian Shield as it consists mainly of juvenile Neoproterozoic crustal material (Alene *et al.* 2000; Beyth *et al.* 2003; Fritz *et al.* 2013). The arc phase is represented by effusive flows and diverse volcaniclastic rocks of the upper Tonian Tsaliet Group (Beyth 1972b; Miller *et al.* 2009). When magmatism ceased, the marine siliciclastic and carbonate succession of the Cryogenian Tambien Group was deposited (Alene *et al.* 2006; Avigad *et al.* 2007; Miller *et al.* 2009). Both units experienced greenschist-facies metamorphism and intrusion of syn- and post-tectonic granitoids and diorites (Beyth 1972b; Kazmin *et al.* 1978; Tefera *et al.* 1996). In western and southern Ethiopia, the basement can be regarded as the transition between the Arabian–Nubian Shield and the Mozambique Belt, as it shows features of both; the crust is mainly juvenile Neoproterozoic with an age range indistinguishable from that of the Arabian–Nubian Shield (Teklay *et al.* 1998; Stern *et al.* 2012). Furthermore, the basement includes a significant proportion of ophiolitic and volcano-sedimentary units (Woldemichael *et al.* 2010; Stern *et al.* 2012). High-grade metamorphic rocks are abundant in western and southern Ethiopia (Yibas *et al.* 2002; Woldemichael *et al.* 2010; Stern *et al.* 2012) and Archaean protoliths were recognised in the Alghae Terrane in southern Ethiopia (Stern *et al.* 2012). The east Ethiopian basement, however, represents a separate crustal domain. Here,

granitoid chemistry, zircon ages and Nd–Sr isotopes point to considerable reworking of pre-Neoproterozoic crust (Teklay *et al.* 1998). These characteristics extend to northern Somalia and maybe even to the southernmost Arabian Peninsula, since similar basement was also found in southern Yemen (Windley *et al.* 1996; Teklay *et al.* 1998).

The Phanerozoic sediment cover in Ethiopia starts with the Upper Ordovician–Lower Silurian Enticho Sandstone. Cambrian or Early Ordovician sediments are missing. The Enticho Sandstone occurs north of the Mekelle Basin (Fig. 2a) and has a thickness of up to 300 m (e.g. Saxena & Assefa 1983; Dawit 2010). It consists of a lower glaciogenic unit and an upper shallow marine unit (Bussert & Dawit 2009). The glaciogenic part comprises massive and large-scale cross-bedded sandstones and conglomerates, assumed to be (subaerial or subaqueous) meltwater deposits. Foreset dips indicate a transport direction towards the south-east (Bussert & Dawit 2009). In places, transport directions are towards the north (Kumpulainen 2007; Bussert & Dawit 2009). Diamictites occur rarely (Bussert & Dawit 2009; Dawit 2010). In the upper part, well-sorted sandstones with bipolar cross-bed sets point to a tide-dominated shallow marine depositional setting (Bussert & Dawit 2009; Dawit 2010). Locally, a mudstone unit separates the glaciogenic and the shallow marine sandstones.

The age of the Enticho Sandstone was constrained by body and trace fossils, as well as palynoflora (cryptospores). Based on fossil siphonophorid impressions, Saxena & Assefa (1983) assigned an Ordovician age. Bussert & Dawit (2009) discovered *Arthrophycus*

alleghaniensis in the upper, shallow-marine unit, an ichnospecies that is largely restricted to the early Silurian (Seilacher 2007; Buatois & Mangano 2011). Additional biostratigraphic evidence comes from recently discovered cryptospores, colonial algae and phosphatic-shelled inarticulate brachiopods from the lower glaciogenic unit of the Enticho Sandstone. These were assigned by Brocke *et al.* (2015) as post-Hirnantian (latest Ordovician–early Silurian).

The Edaga Arbi Glacials are mainly exposed along the western and southwestern margin of the Mekelle Basin and to a minor extent in the Blue Nile region in western Ethiopia (Fig. 2b). In northern Ethiopia, their thickness is up to 200 m, but significant lateral variations occur (Bussert 2010). The Edaga Arbi Glacials lie unconformably on top of the Enticho Sandstone and, in places, directly on the basement (e.g. Beyth 1972b). They are laminated claystones and siltstones containing scattered out-sized clasts, lenses of sandstone, and a polymict glacial conglomerate at the base (Beyth 1972b; Bussert & Dawit 2009; Bussert 2014). The occurrence is often in N–S oriented troughs and channels that carve into the basement with an inferred transport direction from south to north (Bussert 2010). The following model for the generation of this succession is proposed by Bussert (2014): (1) Initial glacier advance leads to the deposition of tillites; (2) During glacial retreat, (subaerial and subaqueous) outwash fans form; (3) In a pro-glacial lake or fjord-like environment fines settle from the water column, interrupted by periodic hyperpycnal sediment flows and the deposition of dropstones. In the Blue Nile region (Fig. 2b), Permian–Triassic continental sedimentary rocks partly overlie the glacial sediments

presumed to be equivalent to the Edaga Arbi Glacials (Dawit 2014). For a more detailed facies description of the Enticho Sandstone and the Edaga Arbi Glacials the reader is referred to Bussert & Dawit (2009), Bussert (2014), and Lewin *et al.* (2018).

The age of the Edaga Arbi Glacials was constrained by the rich and well-preserved microfloral assemblages, including *Potonieisporites* sp., *Plicatipollenites* sp., *Cycadopytes cymbatus*, and *Microbaculispora* sp. (Bussert & Schrank 2007). These palynotaxa are known from the Early Permian glacial sequences across the whole Gondwana region and are used for stratigraphic correlations (e.g. Kemp *et al.* 1977; Backhouse 1991; Stephenson *et al.* 2003).

Methods

Sandstone samples were collected from surface outcrops mainly in northern Ethiopia, where Palaeozoic glaciogenic sedimentary rocks are abundant. In the Blue Nile region, in the west of the country, such sandstones could only be sampled in one locality (Fig. 2b). The choice of sampling sites was based on previous stratigraphic and sedimentological work (Bussert & Schrank 2007; Bussert & Dawit 2009). Four sections were sampled that are biostratigraphically constrained (Bussert & Dawit 2009; Brocke *et al.* 2015). The other sampled sections where assigned to one of the two formations by lithofacies characteristics. The field classification could be confirmed by geochemical analyses, which are well suited to distinguish between the two formations and assign unknown samples (Lewin *et al.* 2018). Eleven samples were chosen for detrital zircon

geochronology, six samples from the Enticho Sandstone and five from the Edaga Arbi Glacials (Table 1). The choice was made in order to cover a large geographic and stratigraphic spread within each formation.

To prepare for zircon analysis, 1–2 kg of each sample was disaggregated using a jaw crusher followed by mortar and pestle, and wet sieved. Heavy minerals were separated from the 63–125 μm grain-size fraction using sodium polytungstate with a density of 2.85 g/mL. We chose this grain-size fraction to ensure comparability with existing data from Palaeozoic sandstones in Libya. Zircon grains were randomly handpicked from the heavy mineral concentrates, mounted in epoxy resin and polished to expose the grains' interior. Cathodoluminescence (CL) images of the grains were taken to reveal the internal structures prior to analysis. We analysed 80 zircons per sample since this appears to produce a robust number of ages for deciphering the sources of natural detrital samples (e.g. Sláma & Košler 2012). For samples Enti-4 and Hu-1, zircon fertility was too low to analyse 80 grains, and only 54 and 47 grains, respectively, could be dated (Table 1). If zircon grains had inherited cores, the measuring spot was set, where possible, on the outer rim, to date always the latest event.

Zircon U–Pb analyses were performed at the Institute of Mineralogy at the University of Münster using a ThermoFisher Element 2 single-collector ICP-MS coupled with a Photon Machines Analyte G2 laser ablation system. Laser spot size was 25 μm. The masses 202 (to determine ^{204}Hg interference with ^{204}Pb), 204, 206, 207 and 238 were measured. Common Pb correction was performed after Stacey &

Kramers (1975) if the common ^{206}Pb fraction of total ^{206}Pb exceeded 1 %. The GJ-1 reference zircon (Jackson *et al.* 2004) was used for calibration by bracketing ten unknowns with three analyses of the reference zircon. To further ensure reproducibility and precision of the U–Pb ages, the 91500 reference zircon (Wiedenbeck *et al.* 1995) was regularly analysed. Measured isotopic ratios match the published values of Wiedenbeck *et al.* (1995).

Data processing was done with an in-house Excel® spreadsheet (Kooijman *et al.* 2012). Due to the lower precision of $^{207}Pb/^{206}Pb$ values for young zircons the data were filtered based on two criteria: (a) agreement in the U–Pb ages (($^{206}Pb/^{238}U$)/($^{207}Pb/^{235}U$)) in the range of 90–110 % for grains younger than 1200 Ma and (b) 90–110 % concordance in terms of ($^{206}Pb/^{238}U$)/($^{207}Pb/^{206}Pb$) for grains older than 1200 Ma. Zircons younger than 1200 Ma were quoted by their $^{206}Pb/^{238}U$ age whereas the $^{207}Pb/^{206}Pb$ age is used for zircons older than 1200 Ma. This age was chosen due to the natural gap of zircon ages in the analysed samples. The R-package 'provenance' (Vermeesch *et al.* 2016) was used for visualisation of the zircon age spectra as kernel density estimates (KDE) and for multi-sample comparison in multidimensional scaling (MDE) maps, as suggested by Vermeesch (2013).

Results

In total, 852 zircon grains were dated in eleven samples from the studied formations, of which 756 were 90–110 % concordant using the respective data filter described above. In the Enticho Sandstone, 481 grains were analysed, of which 421 (88 %) were concordant, and

in the Edaga Arbi Glacials 371 grains, of which 335 (90 %) were concordant (Table 1). Most zircons are prismatic or short prismatic in shape and subrounded to well rounded. In the CL images, they mostly exhibit oscillatory (magmatic) zoning (Fig. 3). Only very few zircons are unzoned and thus probably metamorphic in origin or metamorphically overprinted.

Five main age groups can be defined in detrital zircons of the Enticho Sandstone and the Edaga Arbi Glacials (Figs. 4–6): Pan-African (550–700 Ma), Tonian (700–900 Ma), Stenian–Tonian (900–1200 Ma), Palaeoproterozoic (1600–2500 Ma), and Archaean (>2500 Ma).

The Pan-African population is ubiquitous in both formations and comprises around 40% of the zircon grains. The Tonian age group is very prominent in the Edaga Arbi Glacials (45% of all zircon grains on average), yet less important in the Enticho Sandstone (22% of all zircon grains on average; Fig. 6). An exception is sample Nib-1, which shows a well-defined peak of Tonian aged zircons (Fig. 4). On the other hand, the Stenian–Tonian age population is characteristic for the Enticho Sandstone (Fig. 4 and 6), where it comprises 19% of all ages in contrast to the Edaga Arbi Ages with 5% of the ages in this group.

The ratio of Tonian/Stenian–Tonian ages is on average 1.2 in the Enticho Sandstone (range: 1.0–1.6) and 13.1 in the Edaga Arbi Glacials (range: 5.0–22.0) and can be used to discriminate between the age spectra of both formations. Within the formations, no stratigraphic pattern in zircon age spectra was detected. Mesoproterozoic ages older than Stenian are rare in both formations

and comprise only 5 of the 756 concordant ages. The Palaeoproterozoic and Archaean age populations are more prominent in the Enticho Sandstone than in the Edaga Arbi Glacials. The former contains on average 9% Palaeoproterozoic and 5% Archaean zircons whereas in the latter 4% of the zircons are Palaeoproterozoic and 1% Archaean in age. The proportion of Palaeoproterozoic to Archaean zircons varies with the geographic position of the samples (Fig. 6). Four percent of the zircons in both formations are younger than 550 Ma (Fig. 6).

Discussion

Enticho Sandstone

The largest zircon population in the Enticho Sandstone is of Pan-African age (550–700 Ma; Figs. 4 and 6). Rocks of this age are ubiquitous in the whole East African Orogen and record syn- and post-collisional magmatism associated with the final assembly of Gondwana (e.g. Fritz *et al.* 2013). It is thus hard to assign a particular provenance to these zircons. Of higher interest is the Stenian–Tonian (900–1200 Ma) age group, as it is characteristic for the Enticho Sandstone (Figs. 4 and 6). In the basement of the Arabian–Nubian Shield, zircons of this age are found in Neoproterozoic metasediments in Sinai, the Elat area in southern Israel, and also in Cryogenian diamictites in Ethiopia (Avigad *et al.* 2007; Be'eri-Shlevin *et al.* 2009; Morag *et al*. 2012). Be'eri-Shlevin *et al*. (2009) postulate a tract of *c.* 1 Ga-old crust incorporated in the Arabian–Nubian Shield and conclude a proximal provenance for the upper Neoproterozoic and lower Palaeozoic sediments. Similar

considerations are made by Avigad *et al.* (2007) on the origin of *c.* 1 Ga zircons in the Cryogenian diamictites in Ethiopia. It may thus be possible that the Stenian–Tonian zircon population in the Enticho Sandstone is derived from such metasediments or the postulated former crustal tract. The nearest crust with an age of *c.* 1 Ga still existing in North-East Africa, however, is reported from a) the Central Saharan Belt (Toteu *et al.* 2001; De Wit *et al.* 2005) and b) the Irumide Belt and plutons in the Ubendian Belt, both part of the Mozambique Belt in Tanzania and Mozambique (Bingen *et al.* 2009; De Waele *et al*. 2009; Fritz *et al.* 2013).

According to the super-fan hypothesis (Squire *et al.* 2006; Meinhold *et al.* 2013), *c.* 1 Ga zircons have been transported from regions in the centre of the East African Orogen (i.e. Mozambique Belt) towards the continental margin of Gondwana during the early Palaeozoic. High similarity between the Upper Ordovician–Lower Silurian sandstones in Ethiopia and Libya can be revealed in a multidimensional scaling (MDS) map of the detrital zircon age spectra (Fig. 7). The Algerian Hirnantian sandstone, however, is not part of the cluster. We did not consider age equivalent deposits outside the Gondwana mainland since the palaeogeographic position of the peri-Gondwana terranes is highly uncertain. The differences are mainly in the presence or absence of *c.* 1 Ga zircons, which can be used as a tracer for areas within reach of the super-fan system (Meinhold *et al.* 2013). The boundary between this East African–Arabian zircon province and the West–African province is also illustrated by Linnemann *et al.* (2004) and statistically highlighted by Stephan *et al.* (2019). The remarkable accordance of the detrital

zircon age spectra in sandstone from Libya and Ethiopia makes a common provenance within the Gondwana super-fan system, which lead to regional homogenisation of the detritus, more likely than a derivation of the Stenian–Tonian zircons from the local basement of Ethiopia. When including also zircon ages from older sandstones (Cambrian–Ordovician) of northern Africa in the MDS map (Fig. 8), a spatial clustering appears rather than a temporal. The Enticho Sandstone clusters with Cambrian–Ordovician sandstones from Israel and Jordan, the Libyan sandstones are in the vicinity, and the Algerian and Moroccan are further away in the plot implying least similarity of the age spectra. The high similarity of the Cambrian–Ordovician age spectra with those of the Hirnantian glaciogenic sandstones leads to the assumption that no change in provenance occurred with the onset of glaciation. Rather, the glaciers reworked the sediment delivered by the super-fan system and strongly weathered in the source area or during transport and temporal storage (Garfunkel 2002; Avigad *et al.* 2005). A cannibalisation of pre-Hirnantian sediments by the Hirnantian glaciers is also suggested by Ghienne *et al.* (2018) for the Upper Ordovician sandstones in Morocco, though these cannibalised sediments did probably not belong to the super-fan system (Fig. 8).

Since no Cambrian or Lower to Middle Ordovician sedimentary rocks exist in Ethiopia, the area was probably a site of sediment bypass or erosion during this period and still elevated in the aftermath of the Pan-African Orogeny. If erosion took place, it was probably minor compared to the whole super-fan material: a prominent population of c. 800 Ma zircons, the signature for the

Ethiopian basement, is not present in the super-fan sediments (Meinhold *et al.* 2013). Alternatively, the Ethiopian basement, rich in c. 800 Ma zircons, may have been exhumed only later and covered by a blanket of detrital material that was transported in the super-fan system. The Hirnantian glaciation probably extended eastward to northern Ethiopia, as witnessed by the tillite, from which sample Enti-4 was taken (see also Bussert & Dawit 2009). Through glaciers or ice streams and meltwater, massive amounts of sediment were transported to Ethiopia. Especially during meltdown of the ice sheet, they were released and deposited. The lower part of the Enticho Sandstone is interpreted to represent outwash fan deposits (Bussert & Dawit 2009). The post-glacial transgression provided increased accommodation space to store sediment and to allow deposition of the upper, shallow marine part of the Enticho Sandstone. The original depositional site of the super-fan sediments that were reworked and transported to Ethiopia during the glaciation remains unclear. Assuming an ice spreading centre in mid-northern Africa (e.g. Ghienne *et al.* 2007; Le Heron & Craig 2008), these sediments may have come from the north-west, e.g. the area of Libya. This transport direction would agree with foreset dips towards the south-east as observed in meltwater deposits by Bussert & Dawit (2009).

A considerable population of Palaeoproterozoic to Archaean zircons is present in the Enticho Sandstone (Figs. 4 and 6). Such pre-Neoproterozoic zircons are also detected in increasing amounts up-section in the Cambrian–Ordovician successions in Libya, Israel, and Jordan and are interpreted to record southward migration of river systems associated with the Gondwana super-fan system (Kolodner

et al. 2006; Meinhold *et al.* 2013). Based on Hf isotopic signatures of zircons in Cambrian–Ordovician sandstones in Israel and Jordan, Morag *et al.* (2011) postulated that a large proportion of the material was sourced from ancient terranes outside the Arabian–Nubian Shield. This was recently confirmed by Dor *et al.* (2018) analysing Sr and Nd isotopes in feldspars and clays of such sandstones. This supports a distant provenance of the material in the Enticho Sandstone and recycling of super-fan sediments. However, the proportion of the oldest zircon populations varies with the geographic position of the samples with the highest proportion in samples Nib-1 and Nib-3 (Fig. 6). Hence, it cannot be ruled out that these older zircons are a local phenomenon. Hargrove *et al.* (2006) reported inherited Palaeoproterozoic and Archaean zircons in magmatic rocks of the Arabian–Nubian Shield in Saudi Arabia, which may also be the case in the Ethiopian Neoproterozoic basement.

Avigad *et al.* (2017) analysed detrital rutile U–Pb cooling ages in Cambrian–Ordovician sandstones in Israel and Jordan and one sample from the Enticho Sandstone in Ethiopia. They found younger cooling ages in the Ethiopian sandstone than in the samples from Israel and Jordan and ascribed this to a change in drainage system and supply from new crustal vestiges. The detrital zircon age spectrum of that sample is, however, very similar to the spectra in the Edaga Arbi Glacials (Fig. 5) with a prominent age peak around 800 Ma and only a few *c.* 1 Ga-old zircons leading to a high ratio of Tonian/Stenian–Tonian ages. The Ethiopian sample analysed by Avigad *et al.* (2017) might, therefore, be of Carboniferous–Permian and not of Ordovician–Silurian age.

Edaga Arbi Glacials

Besides the Pan-African (550–700 Ma) "background signal" the Tonian (*c.* 800 Ma) age group is very pronounced in the Carboniferous–Permian Edaga Arbi Glacials (Figs. 5 and 6). This age coincides with the earliest stage of the formation of the Arabian–Nubian Shield when Rodinia broke up. Woldemichael *et al.* (2010) postulated magmatism in western Ethiopia associated with the opening of the Mozambique Ocean and constrained the pulses of magmatism at 860–850 Ma and 795–785 Ma. Kebede *et al*. (2001) dated granitoids of the Western Ethiopian Shield to an age of 815 Ma. In the Southern Ethiopian Shield magmatic episodes at 890–840 Ma and 790–700 Ma, respectively, can be defined (Teklay *et al.* 1998; Yibas *et al.* 2002; Stern *et al.* 2012). They overlap in age with the arc and back-arc magmatism of the Tsaliet Group in northeast Ethiopia and Eritrea (Avigad *et al.* 2007). Johnson *et al.* (2011) assigned protolith ages of 870–840 Ma to the Tokar–Barka terrane in the north Ethiopian–Eritrean basement. Altogether, 700–900 Ma magmatic rocks are abundant in the local and regional basement and are thus the most likely source for the zircons of this age in the Edaga Arbi Glacials. This agrees with earlier considerations of a local provenance for this formation based on sandstone petrography and geochemistry (Lewin *et al.* 2018).

The glaciers of the Late Palaeozoic Ice Age (LPIA) in NE Africa were probably of local, mountain-glacier type (Konert *et al*. 2001; Bussert & Schrank 2007; Le Heron *et al.* 2009). Uplift of the Ethiopian basement likely occurred due to Carboniferous Hercynian

tectonism (Al-Husseini 1992; Sharland *et al.* 2004). On the Arabian Peninsula, this tectonism caused N–S oriented faults, sags and swells (Al-Husseini 2004). The Edaga Arbi Glacials in northern Ethiopia are presumed to have been deposited in a large NNE trending trough in which glacial erosion may have followed and reinforced this pre-glacial topography (Bussert 2014). Another reason for uplift could be thermal updoming prior to the formation of the Zagros rift zone that later formed the Neo-Tethys ocean (Sharland *et al.* 2001). Bussert (2010) studied erosional landforms associated with the LPIA in northern Ethiopia and proposed a landscape of areal scouring, in which wet-based ice carved deeply into the basement. This would have enabled efficient erosion of *c.* 800 Ma zircon-bearing rocks, which can also have provided the rutiles analysed by Avigad *et al.* (2017). In the Enticho Sandstone, sample Nib-1 contains a notable age peak of *c.* 800 Ma as well (Fig. 4). The assignment of this sample to the Enticho Sandstone is through biostratigraphy and is further confirmed by geochemical analysis (Lewin *et al.* 2018) and the ratio of Tonian/Stenian–Tonian zircons of 1.1. This leads to the assumption that locally the Ordovician glaciers were able to erode the local basement effectively due to differences in topography or in glacier dynamics.

Few concordant Phanerozoic zircon ages are present in both studied formations, mainly in the range of 450–520 Ma. Almost all these young zircons are corrected for common Pb, so they may be overcorrected leading to younger ages. However, magmatic activity in the area at that time cannot be excluded either. In Ethiopia, there is no clear evidence for early Palaeozoic magmatism, but Sacchi *et al.*

(2007) identified fresh volcanic clasts in Palaeozoic tillite in northern Ethiopia. Yet, it is doubtful whether this tillite is of Ordovician or Carboniferous–Permian age. In the explanations of the Geological map of the Mekelle area from 1970, a black lava layer is described that lies on top of the basement peneplain and is interpreted to have formed before the Mesozoic (Levitte 1970). Even though it is described as ultrabasic, it may have delivered minor amounts of zircon to the Palaeozoic sediments. In Libya, Middle Ordovician volcanic ash beds (K-bentonites) are reported (Ramos *et al.* 2003) and ascribed to volcanic activity in northern Gondwana during that time. Such volcanic products could have provided an additional or alternative source. Cambrian post-collisional plutons in the Arabian–Nubian Shield are reported by Fritz *et al.* (2013), yet it is unknown whether they were exposed at the times of deposition of the studied formations.

The preservation of mainly glaciation-related sediments in the Palaeozoic of Ethiopia is striking. As an explanation, we propose a combination of increased sediment delivery by glaciers, ice streams, and meltwater, and increased accommodation space at the times of deposition. Towards the end of the Hirnantian glaciation, the melting ice sheet released large amounts of sediment and through the following transgression accommodation space was created in the area of Ethiopia. Afterwards, the isostatic rebound may have caused uplift of the area leading to another period of non-deposition. Sea-level fall has also accompanied Silurian–early Devonian Palaeotethys rifting (Torsvik & Cocks 2011). In the Carboniferous–Permian, Hercynian tectonism produced a complex local geomorphology. Areas that were

uplifted, glaciated and eroded were close to local depressions in which proglacial lakes provided numerous depocentres for sediment accumulation.

A remaining question is, why no major recycling of the Enticho Sandstone by the Edaga Arbi Glacials has taken place. This may be because the deposition of the Enticho Sandstone was limited to northern Ethiopia (Kazmin 1972; Tefera *et al*. 1996). The source area of the Edaga Arbi Glacials was probably to the south: a northward transport direction was inferred by Bussert (2010) based on the orientation and geometry of palaeolandforms such as roches moutonnées. Furthermore, sedimentary rocks presumed to be equivalent to the Edaga Arbi Glacials are also present in the Blue Nile area (samples Hu-1 and Hu-2, showing the same zircon age signature as the other samples from the Edaga Arbi Glacials) and in other parts of Ethiopia (e.g. Bussert & Dawit 2009 and references therein).

Conclusions

The U–Pb dating of detrital zircons in the Upper Ordovician (Hirnantian) to Lower Silurian Enticho Sandstone and the Carboniferous–Permian Edaga Arbi Glacials in northern Ethiopia reveals distinct differences in the age spectra of both formations. Differences exist mainly in the Tonian (700–900 Ma) age population, which is characteristic for the Edaga Arbi Glacials, and the Stenian–Tonian (900–1200 Ma) group, which is prominent in the Enticho

Sandstone. We can, therefore, rule out recycling of the Enticho Sandstone by the Edaga Arbi Glacials on a grand scale.

The Stenian–Tonian zircons are correlative with characteristic populations of this age in Hirnantian sandstones in Libya and Cambrian–Ordovician sandstones in Libya, Israel, and Jordan. Following the hypothesis of a Gondwana super-fan system in the Early Palaeozoic that can be traced by *c.* 1 Ga zircons, the Enticho Sandstone can be regarded as super-fan sediments reworked by the Late Ordovician glaciers and during the subsequent transgression. The Tonian zircon population, which is very prominent in the Carboniferous–Permian Edaga Arbi Glacials, is likely derived from the local basement of Ethiopia. Here, 700–900 Ma magmatic rocks are very abundant and represent the earliest formation stage of the southern Arabian–Nubian Shield. These basement rocks must have been uplifted and exposed for efficient erosion by the glaciers of the Late Palaeozoic Ice Age.

The preservation of mainly glaciation-related sediments in the Palaeozoic of Ethiopia is probably a consequence of 1) high sediment supply due to the erosional and transport potential of glaciers, ice streams, and meltwater, and 2) the creation of accommodation space during these times. For the Enticho Sandstone, the latter resulted from base-level rise due to post-glacial transgression that reached southward (in present-day coordinates) as far as Ethiopia. For the Edaga Arbi Glacials, accommodation space was created in proglacial lakes in local depressions. Since the deposition of the Enticho Sandstone was probably limited to northern Ethiopia and the inferred

source area of the Edaga Arbi Glacials is to the south, no major recycling of the former by the latter took place.

Acknowledgements and Funding

This work was funded by the German Research Foundation (DFG grants HI 643/13-1, ME 3882/4-1). We are grateful to A. Kronz for providing access to the electron microprobe for CL imaging, and to B. Schmitte for assistance at the LA-ICP-MS facility. This paper benefited from careful reviews by W. Bosworth and D. P. Le Heron.

References

Alene, M., Jenkin, G.R.T., Leng, M.J. & Darbyshire, D.P.F. 2006. The Tambien Group, Ethiopia: An early Cryogenian (ca. 800–735 Ma) Neoproterozoic sequence in the Arabian–Nubian Shield. *Precambrian Research*, **147**, 79–99.

Alene, M., Ruffini, R. & Sacchi, R. 2000. Geochemistry and Geotectonic Setting of Neoproterozoic Rocks from Northern Ethiopia (Arabian-Nubian Shield). *Gondwana Research*, **3**, 333–347.

Al-Husseini, M.I., 1992. Upper Palaeozoic tectono-sedimentary evolution of the Arabian and adjoining plates. *Journal of the Geological Society, London,* **149**, 419–429.

Al-Husseini, M.I., 2004. Pre-Unayzah unconformity, Saudi Arabia. In: Al-Husseini, M.I. (Ed.), Carboniferous, Permian and Early Triassic Arabian Stratigraphy. *GeoArabia, Special Publication,* **3**, 15–59.

Altumi, M.M., Elicki, O., Linnemann, U., Hofmann, M., Sagawe, A. & Gärtner, A. 2013. U–Pb LA-ICP-MS detrital zircon ages from the Cambrian of Al Qarqaf Arch, central-western Libya: Provenance of the West Gondwanan sand sea at the dawn of the early Palaeozoic. *Journal of African Earth Sciences*, **79**, 74–97.

Arkin, Y., Beyth, M., Dow, D.B., Levitte, D., Temesgen, H. & Tsegaye, H. 1971. *Geological map of Mekele area*, sheet ND 37-11. Geological survey of Ethiopia, Addis Abeba, scale: 1:250000.

Avigad, D., Gerdes, A., Morag, N. & Bechstädt, T. 2012. Coupled U–Pb–Hf of detrital zircons of Cambrian sandstones from Morocco and Sardinia: Implications for provenance and Precambrian crustal evolution of North Africa. *Gondwana Research*, **21,** 690–703.

Avigad, D., Morag, N., Abbo, A. & Gerdes, A. 2017. Detrital rutile U-Pb perspective on the origin of the great Cambro-Ordovician sandstone of North Gondwana and its linkage to orogeny. *Gondwana Research*, **51,** 17–29.

Avigad, D., Sandler, A., Kolodner, K., Stern, R., McWilliams, M., Miller, N. & Beyth, M. 2005. Mass-production of Cambro–Ordovician quartz-rich sandstone as a consequence of chemical weathering of Pan-African terranes: Environmental implications. *Earth and Planetary Science Letters*, **240**, 818–826.

Avigad, D., Stern, R.J., Beyth, M., Miller, N. & McWilliams, M.O. 2007. Detrital zircon U–Pb geochronology of Cryogenian diamictites and Lower Paleozoic sandstone in Ethiopia (Tigrai): Age constraints on Neoproterozoic glaciation and crustal evolution of the southern Arabian–Nubian Shield. *Precambrian Research*, **154,** 88–106.

Be'eri-Shlevin, Y., Katzir, Y., Whitehouse, M.J. & Kleinhanns, I.C. 2009. Contribution of pre Pan-African crust to formation of the Arabian Nubian Shield: New secondary ionization mass spectrometry U-Pb and O studies of zircon. *Geology*, **37**, 899–902.

Beyth, M. 1972a. Paleozoic-Mesozoic sedimentary basin of the Mekele Outlier, Northern Ethiopia. *AAPG Bulletin*, **56,** 2426–2439.

Beyth, M. 1972b. *To the geology of central-western Tigre*. PhD thesis, Rheinische Friedrich-Wilhelms-Universität Bonn, Bonn.

Beyth, M., Avigad, D., Wetzel, H.U., Matthews, A. & Berhe, S.M. 2003. Crustal exhumation and indications for Snowball Earth in the East African Orogen: north Ethiopia and east Eritrea. *Precambrian Research*, **123,** 187–201.

Bingen, B., Jacobs, J., Violaa, G., Hendersona, I.H.C., Skåra, Ø., Boyda, R., Thomasc, R.J., Solli, A., Keyc, R.M. & Daudid, E.X.F. 2009. Geochronology of the Precambrian crust in the Mozambique belt in NE Mozambique, and implications for Gondwana assembly. *Precambrian Research*, **170**, 231–255.

Backhouse, J. 1991. Permian palynostratigraphy of the Collie Basin, Western Australia. *Review of Palaeobotany and Palynology* **67**, 237-314.

Brocke, R., Bussert, R., Dawit, E.L. 2015. First discovery of Early Palaeozoic post-glacial (post-Hirnanatian/latest Ordovician–early Silurian) mudstones and cryptospores in northern Ethiopia. In: Wagner, J., Elger, K. (eds.) GeoBerlin 2015—Dynamic Earth from Alfred Wegener to today and beyond—Abstracts. Annual Meeting of DGGV and DMG, 4–7 October 2015, Berlin: GFZ German Research Centre for Geosciences, p. 100.
DOI: http://doi.org/10.2312/GFZ.LIS.2015.003.

Buatois, L. A., Mángano, M. G. 2011. Ichnology: Organism–Substrate Interactions in Space and Time. Cambridge University Press, Cambridge, 358 pp.

Burke, K., MacGregor, D.S. & Cameron, N.R. 2003. Africa's petroleum systems: four tectonic 'Aces' in the past 600 million years. *In:* T.J. Arthur, D.S. MacGregor & N.R. Cameron (eds.) *Petroleum Geology of Africa: new themes and developing technologies*. Geological Society, London, Special Publication, **207**, 21–60.

Bussert, R. 2010. Exhumed erosional landforms of the Late Palaeozoic glaciation in northern Ethiopia: Indicators of ice-flow direction, palaeolandscape and regional ice dynamics. *Gondwana Research*, **18,** 356–369.

Bussert, R. 2014. Depositional environments during the Late Palaeozoic ice age (LPIA) in northern Ethiopia, NE Africa. *Journal of African Earth Sciences*, **99**, 386–407.

Bussert, R. & Dawit, E.L. 2009. Unexpected diversity: New results on the stratigraphy and sedimentology of Palaeozoic and Mesozoic siliciclastic sediments in Northern Ethiopia. *Zentralblatt für Geologie und Paläontologie*, **Teil I(3/4)**, 181–198.

Bussert, R.& Schrank, E. 2007. Palynological evidence for a latest Carboniferous-Early Permian glaciation in Northern Ethiopia. *Journal of African Earth Sciences*, **49,** 201–210.

Collins, A.S. & Pisarevsky, S.A. 2005. Amalgamating eastern Gondwana: The evolution of the Circum-Indian Orogens. *Earth-Science Reviews*, **71,** 229–270.

Dawit, E.L. 2010. *Adigrat Sandstone in Northern and Central Ethiopia: Stratigraphy, Facies, Depositional Environments and Palynology*. PhD thesis, Berlin Technical University, Berlin.

Dawit, E.L. 2014. Permian and Triassic microfloral assemblages from the Blue Nile Basin, central Ethiopia. *Journal of African Earth Sciences*, **99,** 408–426.

De Waele, B., Fitzsimons, I.C.W., Wingate, M.T.D., Tembo, F.,

Mapani, B. & Belousova, A. 2009. The geochronological framework of the Irumide Belt: A prolonged crustal history along the margin of the Bangweulu Craton. *American Journal of Science*, **309,** 132–187.

De Wit, M.J., Bowring, S.A., Dudas, F. & Kamga, G. 2005. The great Neoproterozoic central Saharan Arc and the amalgamation of the North African Shield. *GAC-MAC-CSPG-CSSS Joint Meeting*, Halifax, Nova Scotia, 42–43.

Dor, Y.B., Harlavan, Y. & Avigad, D. 2018. Provenance of the great Cambrian sandstone succession of northern Gondwana unravelled by strontium, neodymium and lead isotopes of feldspars and clays. *Sedimentology*, **65**, 2595–2620.

Dow, D.B., Beyth, M. & Hailu, T. 1971. Palaeozoic glacial rocks recently discovered in northern Ethiopia. *Geological Magazine*, **108,** 53–60.

Eyles, N. 1993. Earth's glacial record and its tectonic setting. *Earth-Science Reviews*, **35,** 1–248.

Fielding, C.R., Frank, T.D. & Isbell, J.L. 2008. The late Paleozoic ice age—A review of current understanding and synthesis of

global climate patterns. *In*: Fielding, C.R., Frank, T.D. & Isbell, J.L. (eds.) *Resolving the Late Paleozoic ice age in time and space*. Geological Sciety of America, Special Papers **441**, 343–354.

Fritz, H., Abdelsalam, M., Ali, K.A., Bingen, B., Collins, A.S., Fowler, A.R., Ghebreab, W., Hauzenberger, C.A., Johnson, P.R., Kusky, T.M., Macey, P., Muhongo, S., Stern, R.J. & Viola G. 2013. Orogen styles in the East African Orogen: A review of the Neoproterozoic to Cambrian tectonic evolution. *Journal of African Earth Sciences*, **86**, 65–106.

Garfunkel, Z. 2002. Early Paleozoic sediments of NE Africa and Arabia: Products of continental-scale erosion, sediment transport and deposition. *Israel Journal of Earth Sciences*, **51**, 135–156.

Garland, C.R., Akililu, A., Assefa, A., Amenti, A., Beyth, M., Dow, D.B., Temesgen, H. & Tsegaye, H. 1978. Geological map of Adigrat, sheet ND 37-7. Geological Survey of Ethiopia Addis Abeba, Scale: 1:250000.

Ghienne, J.-F., Le Heron, D.P., Moreau, J., Denis, M. & Deynoux, M. 2007. The Late Ordovician glacial sedimentary system of the North Gondwana platform. *In*: M.J. Hambrey, P. Christoffersen, N.F. Glasser & B. Hubbard (eds.) *Glacial Sedimentary Processes and Products*. International Association of Sedimentologists Special Publication **39**, 295–319.

Ghienne, J.-F, Benvenuti, A., El Houicha, M., Girard, F., Kali, E., Khoukhi, Y., Langbour, C., Magna, T., Míková, J., Moscariello, A. & Schulmann, K. 2018. The impact of the end-Ordovician glaciation on sediment routing systems: A case study from the Meseta (northern Morocco). *Gondwana Research*, **63**, 169–178.

Hargrove, U.S., Stern, R.J., Kimura, J.I., Manton, W.I. & Johnson, P.R. 2006. How juvenile is the Arabian–Nubian Shield? Evidence from Nd isotopes and pre-Neoproterozoic inherited zircon in the Bi'r Umq suture zone, Saudi Arabia. *Earth and Planetary Science Letters*, **252,** 308–326.

Isbell, J.L., Henry, L.C., Gulbranson, E.L., Limarino, C.O., Fraiser, M.L., Koch, Z.J, Ciccioli, P.L. & Dineen, A.A. 2012. Glacial paradoxes during the late Paleozoic ice age: Evaluating the equilibrium line altitude as a control on glaciation. *Gondwana Research*, **22**, 1–19.

Jackson, S.E., Pearson, N.J., Griffin, W.L. & Belousova, E.A. 2004. The application of laser ablation-inductively coupled plasma-mass spectrometry to in situ U–Pb zircon geochronology. *Chemical Geology*, **211,** 47–69.

Johnson, P.R., Andresen, A., Collins, A.S., Fowler, A.R., Fritze, H., Ghebreab, W., Kusky, T. & Stern, R.J. 2011. Late Cryogenian–Ediacaran history of the Arabian–Nubian Shield: A review of depositional, plutonic, structural, and tectonic events in the closing stages of the northern East African Orogen. *Journal of African Earth Sciences*, **61,** 167–232.

Kazmin, V. 1972. *Geological Map of Ethiopia*. Geological Survey of Ethiopia, Addis Abeba.

Kazmin, V., Shifferaw, A. & Balcha, T. 1978. The Ethiopian basement: Stratigraphy and possible manner of evolution. *Geologische Rundschau*, **67,** 531–546.

Kebede, T., Kloetzli, U.S. & Koeberl, C. 2001. U/Pb and Pb/Pb zircon ages from granitoid rocks of Wallagga area: constraints on magmatic and tectonic evolution of Precambrian rocks of western Ethiopia. *Mineralogy and Petrology*, **71**, 251–271.

Kemp, E.M., Balme, B.E., Helby, R.J., Kyle, R.A., Playford, G. & Price, P.L. 1977. Carboniferous and Permian palynostratigraphy in Australia and Antarctica, a review. *BMR Journal of Australian Geology and Geophysics* **2**, 177–208.

Kolodner, K., Avigad, D., McWilliams, M., Wooden, J.L., Weissbrod, T. & Feinstein, S. 2006. Provenance of north Gondwana Cambrian–Ordovician sandstone: U–Pb SHRIMP dating of detrital zircons from Israel and Jordan. *Geological Magazine*, **143,** 367–391.

Konert, G., Afifi, A.M., Al-Hajri, S.A. & Droste, H.J. 2001. Paleozoic stratigraphy and hydrocarbon habitat of the Arabian Plate. *GeoArabia*, **6**, 407–442.

Kooijman, E., Berndt, J. & Mezger, K. 2012. U-Pb dating of zircon by laser ablation ICP-MS: recent improvements and new insights. *European Journal of Mineralogy*, **24,** 5–21.

Kröner, A., Muhongo, S., Hegner, E. & Wingate, M.T.D. 2003. Single-zircon geochronology and Nd isotopic systematics of Proterozoic high-grade rocks from the Mozambique belt of southern Tanzania (Masasi area): implications for Gondwana assembly. *Journal of the Geological Society, London*, **160**, 745–757.

Kumpulainen, R.A. 2007. The Ordovician glaciation in Eritrea and Ethiopia. *In:* Hambrey, M.J., Christoffersen, P., Glasser, N.F & Hubbard B. (eds.) *Glacial Sedimentary Processes and Products*. International Association of Sedimentologists Special Publication **39**, 321–342.

Kumpulainen, R.A., Uchman, A., Woldehaimanot, B., Kreuser, T. & Ghirmay, S. 2006. Trace fossil evidence from the Adigrat Sandstone for an Ordovician glaciation in Eritrea, NE Africa. *Journal of African Earth Sciences*, **45,** 408–420.

Le Heron, D.P. & Craig, J. 2008. First-order reconstructions of a Late Ordovician Saharan ice sheet. *Journal of the Geological Society, London*, **165,** 19–29.

Le Heron, D.P., Craig, J. & Etienne, J.L. 2009. Ancient glaciations and hydrocarbon accumulations in North Africa and the Middle East. *Earth-Science Reviews*, **93**, 47–76.

Le Heron, D.P., Tofaif, S. & Melvin, J. 2018. The Early Palaeozoic glacial deposits of Gondwana: overview, chronology and controversies. *In:* Menzies, J. & van der Meer, J.J.M. (eds.) *Past Glacial Environments*. 2nd edition, Elsevier, Amsterdam, 47–73.

Levitte, D. 1970. *The Geology of Mekele*. Report on the geology of the central part of sheet ND 37-11, Addis Abeba.

Lewin, A., Meinhold, G., Hinderer, M., Dawit, E.L. & Bussert, R. 2018. Provenance of sandstones in Ethiopia during Late Ordovician and Carboniferous–Permian Gondwana

glaciations: Petrography and geochemistry of the Enticho Sandstone and the Edaga Arbi Glacials. *Sedimentary Geology*, **375,** 188–202.

Linnemann, U., McNaughton, N.J., Romer, R.L., Gehmlich, M., Drost, K. & Tonk, C., 2004. West African provenance for Saxo-Thuringia (Bohemian Massif): Did Armorica ever leave pre-Pangean Gondwana? ? U/Pb-SHRIMP zircon evidence and the Nd-isotopic record. *International Journal of Earth Sciences*, **93**, 683–705.

Linnemann, U., Ouzegane, K., Drareni, A., Hofmann, M., Becker, S., Gärtner, A. & Sagawe, A. 2011. Sands of West Gondwana: An archive of secular magmatism and plate interactions — A case study from the Cambro-Ordovician section of the Tassili Ouan Ahaggar (Algerian Sahara) using U–Pb–LA-ICP-MS detrital zircon ages. *Lithos*, **123**, 188–203.

Mänttäri, I. 2014. Mesoarchaean to Neoproterozoic U-Pb and Sm-Nd ages from Uganda. *In:* Lehto, T., Katto, E. (eds.) *GTK Consortium Geological Surveys in Uganda 2008−2012*. Geological Survey of Finland, Special Paper **56**, 121–164.

Meinhold, G., Morton, A.C. & Avigad, D. 2013. New insights into peri-Gondwana paleogeography and the Gondwana super-fan system from detrital zircon U–Pb ages. *Gondwana Research*, **23**, 661–665.

Meinhold, G., Morton, A.C., Fanning, C.M., Frei, D., Howard, J.P., Richard J. Phillips, R.J., Strogen, D. & Whitham, A.G. 2011. Evidence from detrital zircons for recycling of Mesoproterozoic and Neoproterozoic crust recorded in Paleozoic and Mesozoic sandstones of southern Libya. *Earth and Planetary Science Letters*, **312**, 164–175.

Miller, N.R., Stern, R.J., Avigad, D., Beyth, M. & Schilman, B. 2009. Cryogenian slate-carbonate sequences of the Tambien Group, Northern Ethiopia (I): Pre-"Sturtian" chemostratigraphy and regional correlations. *Precambrian Research*, **170,** 129–156.

Morag, N., Avigad, D., Gerdes, A., Belousova, E. & Harlavan, Y. 2011. Detrital zircon Hf isotopic composition indicates long-distance transport of North Gondwana Cambrian–Ordovician sandstones. *Geology*, **39,** 955–958.

Morag, N., Avigad, D., Gerdes, A. & Harlavan, Y. 2012. 1000–580 Ma crustal evolution in the northern Arabian-Nubian Shield revealed by U–Pb–Hf of detrital zircons from late Neoproterozoic sediments (Elat area, Israel). *Precambrian Research*, **208,** 197–212.

Morton, A.C., Whitham, A., Howard, J., Fanning, M., Abutarruma, Y., El Dieb, M., Elkatarry, F.M., Hamhoom, A.M., Lüning, S., Phillips, R. & Thusu, B. 2012. Using heavy minerals to test the stratigraphic framework of Al Kufrah Basin. *In:* Salem, M.J. & Abadi, A.M. (eds.) *Fourth Symposium on the Sedimentary Basins of Libya. The Geology of Southern Libya*. Earth Science Society of Libya, Tripoli, **3,** 33–76.

Ramos, E., Navidad, M., Marzo, M. & Bolatti, N. 2003. Middle-Ordovician K-bentonite beds in the Murzuq Basin (Central Libya). *In:* Albanesi, G.L., Beresi, M.S. & Peralta S.H (eds.) *Ordovician from the Andes*, Instituto Superior de Correlación Geológica, **17**, 203–207.

Sacchi, R., Alene, M., Barbieri, M. & Conti, A. 2007. On the Palaeozoic Tillite of the Adigrat Group (Tigrai, Ethiopia). *Periodico di Mineralogia*, **76,** 241–251.

Saxena, G.N. & Assefa, G. 1983. New evidence on the age of the glacial rocks of northern Ethiopia. *Geological Magazine*, **120**, 549–554.

Seilacher, A., 2007. Trace Fossil Analysis. Springer Verlag, Berlin, 226 pp.

Sharland, P.R., Archer, R., Casey, D.M., Davies, R.B., Hall, S.H., Heward, A.P., Horbury, A.D. & Simmons, M.D. 2001. Arabian Plate Sequence Stratigraphy. *GeoArabia, Special Publication*, **2**, Gulf PetroLink, Bahrain.

Sharland, P.R., Casey, D.M., Davies, R.B., Simmons, M.D., Sutcliffe, O.E., 2004. Arabian plate sequence stratigraphy revisions to SP2. *GeoArabia* **9**, 199–214.

Shaw, J., 1975. Sedimentary successions in Pleistocene ice-marginal lakes. *In:* Jopling, A.V. & McDonald, B.C. (eds.) *Glaciofluvial and glaciolacustrine sedimentation*, Society of Economic Paleontologists and Mineralogists, Special Publication, **23**, 281–303.

Sláma, J. & Košler, J. 2012. Effects of sampling and mineral separation on accuracy of detrital zircon studies. *Geochemistry, Geophysics, Geosystems*, **13**, 1–17.

Squire, R.J., Campbell, I.H., Allen, C.M. & Wilson, C.J.L. 2006. Did the Transgondwanan Supermountain trigger the explosive radiation of animals on Earth? *Earth and Planetary Science Letters*, **250,** 116–133.

Stacey, J.S. & Kramers, J.D. 1975. Approximation of terrestrial lead isotope evolution by a two-stage model. *Earth and Planetary Science Letters*, **26**, 207–221.

Stephan, T., Kroner, U. & Romer, R.L. 2019. The pre-orogenic detrital zircon record of the Peri-Gondwanan crust. *Geological Magazine*, **156**, 281–307.

Stephenson, M.H., Osterloff, P.L. & Filatoff, J. 2003. Palynological biozonation of the Permian of Oman and Saudi Arabia: progress and challenges. *GeoArabia* **8**, 467–496.

Stern, R.J. 1994. Arc assembly and continental collision in the Neoproterozoic East African Orogen: Implications for the consolidation of Gondwanaland. *Annual Review of Earth and Planetary Sciences*, **22,** 319–351.

Stern, R.J. 2008. Neoproterozoic crustal growth: The solid Earth system during a critical episode of Earth history. *Gondwana Research*, **14,** 33–50.

Stern, R.J., Ali, K.A., Abdelsalam, M.G., Wilde, S.A. & Zhou, Q. 2012. U–Pb zircon geochronology of the eastern part of the Southern Ethiopian Shield. *Precambrian Research*, **206**, 159–167.

Tefera, M., Chernet, T. & Haro, W. 1996. *Explanation of the geological map of Ethiopia*. T.F.D.R.o. Ethiopia, Ministry of Mines and Energy Bulletin.

Teklay, M., Kröner, A., Mezger, K. & Oberhänsli, R. 1998. Geochemistry, Pb-Pb single zircon ages and Nd-Sr isotope composition of Precambrian rocks from southern and eastern Ethiopia: implications for crustal evolution in East Africa. *Journal of African Earth Sciences*, **26**, 207–227.

Torsvik, T.H. & Cocks, L.R.M. 2011. The Palaeozoic palaeogeography of central Gondwana. In: Van Hinsbergen, D. J. J., Buiter, S. J. H., Torsvik, T. H., Gaina, C. & Webb, S. J. (eds) The Formation and Evolution of Africa: A Synopsis of 3.8 Ga of Earth History. *Geological Society, London, Special Publications*, **357**, 137–166.

Torsvik, T.H. & Cocks, L.R.M. 2013. Gondwana from top to base in space and time. *Gondwana Research*, **24**, 999–1030.

Toteu, S.F., Van Schmus, W.R., Penaye, J. & Michard, A. 2001. New U–Pb and Sm–Nd data from north-central Cameroon and its bearing on the pre-Pan African history of central Africa. *Precambrian Research*, **108**, 45–73.

Tsige, L. & Hailu, F. 2007. *Geological Map of the Bure Area*, Ministry of Mines and Energy, Geological Survey of Ethiopia Memoir, Addis Abeba.

Vermeesch, P. 2013. Multi-sample comparison of detrital age distributions. *Chemical Geology*, **341**, 140–146.

Vermeesch, P., Resentini, A. & Garzanti, E. 2016. An R package for statistical provenance analysis. *Sedimentary Geology*, **336**, 14–25.

Wiedenbeck, M., Allé, P., Corfu, F., Griffin, W.L., Meier, M., Oberli, F., von Quadt, A., Roddick, J.C. & Spiegel, W. 1995. Three natural zircon standards for U-Th-Pb, Lu-Hf, trace element and REE analyses. *Geostandards Newsletter*, **19**, 1–23.

Windley, B.F., Whitehouse, M.J. & Ba-Bttat, M.A.O. 1996. Early Precambrian gneiss terranes and Pan-African island arcs in Yemen: Crustal accretion of the eastern Arabian Shield. *Geology*, **24**, 131–134

Woldemichael, B.W., Kimura, J.-I., Dunkley, D.J., Tani, K. & Ohira, H. 2010. SHRIMP U–Pb zircon geochronology and Sr–Nd isotopic systematic of the Neoproterozoic Ghimbi-Nedjo mafic to intermediate intrusions of Western Ethiopia: a record of passive margin magmatism at 855 Ma? *International Journal of Earth Sciences*, **99**, 1773–1790.

Yibas, B., Reimold, W.U., Armstrong, R., Koeberl, C., Anhaeusser, C.R. & Phillips, D. 2002. The tectonostratigraphy, granitoid geochronology and geological evolution of the Precambrian of southern Ethiopia. *Journal of African Earth Sciences*, **34**, 57–84.

Tables

Table 1. Sample information. Locations are given in geographic coordinates (WGS84). The stratigraphic assignment to one of the two studied formations is based on biostratigraphic evidence (B) or lithofacial characteristics (LF) in the outcrop or, in one case, uncertain (U). Detailed information on the petrography and geochemistry of each sample are given in Lewin et al. (2018). Last three columns: summary of detrital zircon ages of samples analysed in this study. The full data set is given as supplementary material.

Figure captions

Fig. 1. (a) Map of Gondwana showing the overall geological setting (modified after Torsvik & Cocks 2013). (b) Map of Eastern Africa and Arabia showing exposures of Precambrian rocks and major tectonic units (modified after Fritz *et al.* 2013). B, Bangweulu; CC, Congo Craton; IB, Irumide Belt; SES, Southern Ethiopian Shield; TC, Tanzania Craton; UB, Ubendian Belt; US, Usagaran Belt; WES, Western Ethiopian Shield; WG, Western Granulite Belt; ZKC, Zimbabwe-Kalahari Craton. Literature for age information: (a) Teklay *et al*. (1998), (b) Woldemichael *et al.* (2010), (c) Kebede *et al.* (2001), (d) Kröner *et al.* (2003), (e) Bingen *et al.* (2009), (f) Mänttäri (2014), (g) Fritz *et al.* (2013), (h) Johnson *et al.* (2011).

Fig. 2. Maps of the study areas showing the sampling locations. (a) Northern Ethiopia (modified after Arkin *et al.* 1971; Garland 1978; Bussert 2014). (b) Blue Nile region (modified after Tsige & Hailu 2007; Dawit 2014). The term "Fincha Sandstone" is taken from Dawit (2014).

Fig. 3. Cathodoluminescence images of representative zircons of the defined age groups. Pan-African: 550–700 Ma, Tonian: 700–900 Ma, Stenian–Tonian: 900–1200 Ma, Palaeoproterozoic: 1600–2500 Ma, Archaean: >2500 Ma.

Fig. 4. Kernel density estimate (KDE) plots of the zircon age spectra in samples of the Enticho Sandstone. Inlet shows a close-up of the 500–1300 Ma age range. Samples are arranged from left to right according to their geographic location from south to north with the lower row from the glaciogenic basal part of the formation and the upper row from the shallow marine upper part.

Fig. 5. Kernel density estimate (KDE) plots of the zircon age spectra in samples of the Edaga Arbi Glacials. Inlet shows a close-up of the 500–1300 Ma age range. Samples are arranged from left to right according to their geographic location from south to north with the lower row from the basal part of the formation and the upper row from the middle to upper part.

Fig. 6. Bar chart showing the distribution of the defined age groups in the analysed samples. Samples of the respective formation are arranged from bottom to top according to their geographic location from south to north.

Fig. 7. Nonmetric multidimensional scaling (MDS) map for the Ordovician–Silurian period. Only Precambrian ages (>541 Ma) are used here due to the low reliability of younger ages (see discussion section for details). Literature data: (a) Linnemann *et al.* (2011), (b) Morton *et al.* (2012), (c) Meinhold *et al.* (2011).

Fig. 8. Nonmetric multidimensional scaling (MDS) map comparing the detrital zircon age spectra of Ordovician–Silurian sandstones analysed in this study with data from Ordovician–Silurian as well as Cambrian–Lower Ordovician sandstones in the literature. Only Precambrian ages (>541 Ma) are used here due to the low reliability of younger ages (see discussion section for details). (a) Meinhold *et al.* (2011), (b) Morton *et al.* (2012), (c) Linnemann *et al.* (2011), (d) Kolodner *et al.* (2006), (e) Altumi *et al.* (2013), (f) Avigad *et al.* (2012). Note that literature data are those compiled by Meinhold *et al.* (2013) augmented by those from (e).

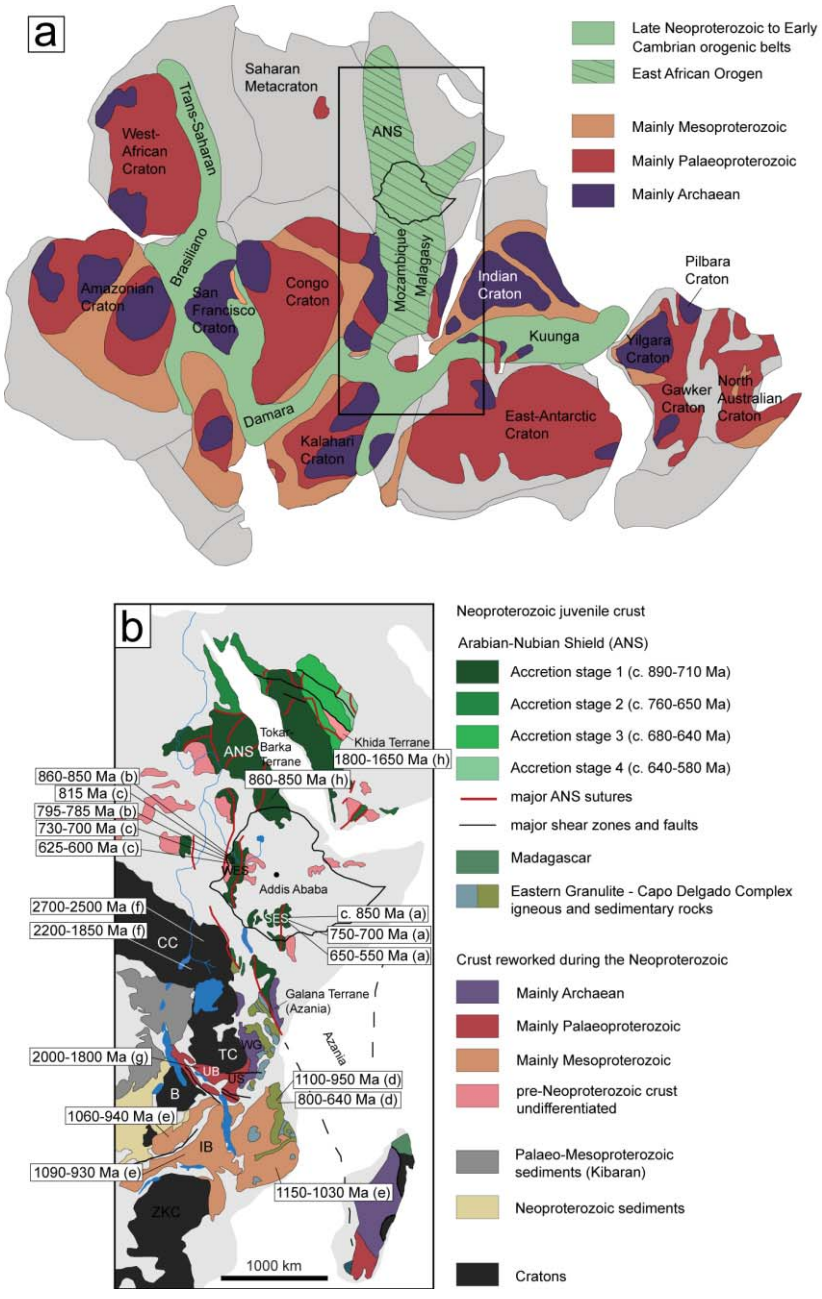
a
Late Neoproterozoic to Early Cambrian orogenic belts
East African Orogen
Mainly Mesoproterozoic
Mainly Palaeoproterozoic
Mainly Archaean
Saharan Metacraton
West-African Craton
Trans-Saharan
ANS
Brasiliano
Amazonian Craton
San Francisco Craton
Congo Craton
Mozambique
Malagasy
Indian Craton
Pilbara Craton
Kuunga
Yilgara Craton
Gawker Craton
North Australian Craton
Damara
Kalahari Craton
East-Antarctic Craton
b
Neoproterozoic juvenile crust
Arabian-Nubian Shield (ANS)
Accretion stage 1 (c. 890-710 Ma)
Accretion stage 2 (c. 760-650 Ma)
Accretion stage 3 (c. 680-640 Ma)
Accretion stage 4 (c. 640-580 Ma)
major ANS sutures
major shear zones and faults
Madagascar
Eastern Granulite - Capo Delgado Complex igneous and sedimentary rocks
Crust reworked during the Neoproterozoic
Mainly Archaean
Mainly Palaeoproterozoic
Mainly Mesoproterozoic
pre-Neoproterozoic crust undifferentiated
Palaeo-Mesoproterozoic sediments (Kibaran)
Neoproterozoic sediments
Cratons
ANS
Khida Terrane
1800-1650 Ma (h)
860-850 Ma (h)
860-850 Ma (b)
815 Ma (c)
795-785 Ma (b)
730-700 Ma (c)
625-600 Ma (c)
MSS
Addis Ababa
SESS
c. 850 Ma (a)
750-700 Ma (a)
650-550 Ma (a)
2700-2500 Ma (f)
2200-1850 Ma (f)
CC
Galana Terrane (Azania)
Azania
WG
TC
UB
US
2000-1800 Ma (g)
1100-950 Ma (d)
800-640 Ma (d)
B
1060-940 Ma (e)
IB
1090-930 Ma (e)
1150-1030 Ma (e)
ZKC
1000 km

Figure 1

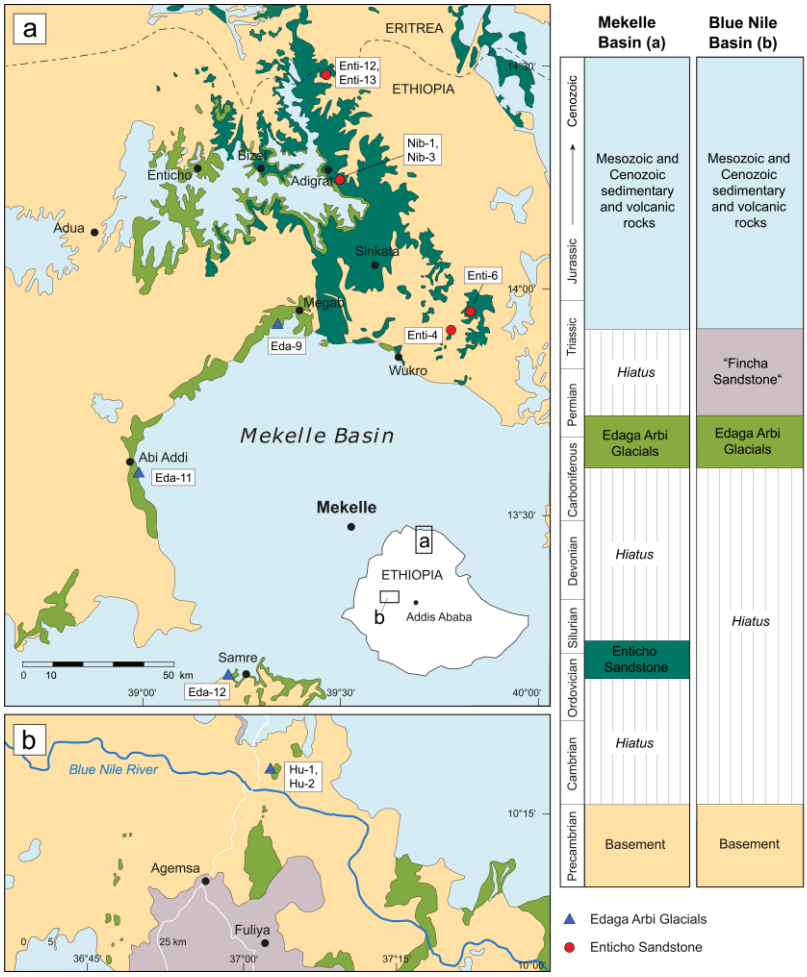
a
ERITREA
ETHIOPIA
Enti-12
Enti-13
Nib-1,
Nib-3
Bizet
Enticho
Adigrat
Adua
Sinkata
Enti-6
Megab
Eda-9
Enti-4
Wukro
Mekelle Basin
Abi Addi
Eda-11
Mekelle
13°30'
a
ETHIOPIA
b
Addis Ababa
Samre
0 10 50 km
39°00'
Eda-12
39°30'
40°00'
14°00'
b
Blue Nile River
Hu-1,
Hu-2
10°15'
Agemsa
Fuliya
0 5 25 km
36°45'
37°00'
37°15'
10°00'
Mekelle Basin (a)
Blue Nile Basin (b)
Cenozoic
Jurassic
Triassic
Permian
Carboniferous
Devonian
Silurian
Ordovician
Cambrian
Precambrian
Mesozoic and Cenozoic sedimentary and volcanic rocks
Mesozoic and Cenozoic sedimentary and volcanic rocks
Hiatus
"Fincha Sandstone"
Edaga Arbi Glacials
Edaga Arbi Glacials
Hiatus
Hiatus
Enticho Sandstone
Hiatus
Basement
Basement
Edaga Arbi Glacials
Enticho Sandstone

Figure 2

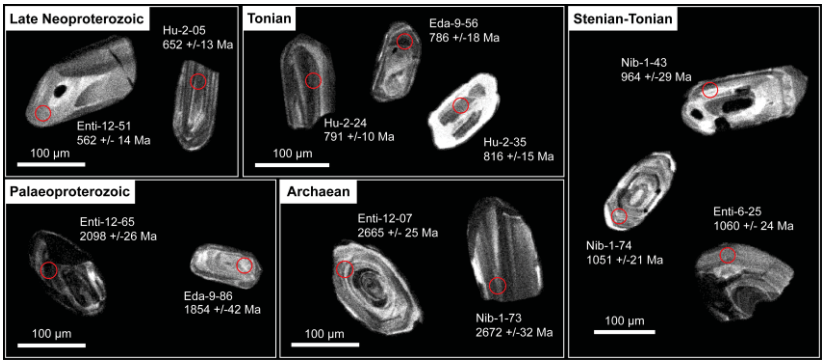
Late Neoproterozoic
Hu-2-05
652 +/-13 Ma
Enti-12-51
562 +/- 14 Ma
100 µm
Tonian
Eda-9-56
786 +/-18 Ma
Hu-2-24
791 +/-10 Ma
Hu-2-35
816 +/-15 Ma
100 µm
Stenian-Tonian
Nib-1-43
964 +/-29 Ma
Enti-6-25
1060 +/- 24 Ma
Nib-1-74
1051 +/-21 Ma
100 µm
Palaeoproterozoic
Enti-12-65
2098 +/-26 Ma
Eda-9-86
1854 +/-42 Ma
100 µm
Archaean
Enti-12-07
2665 +/- 25 Ma
Nib-1-73
2672 +/-32 Ma
100 µm

Figure 3

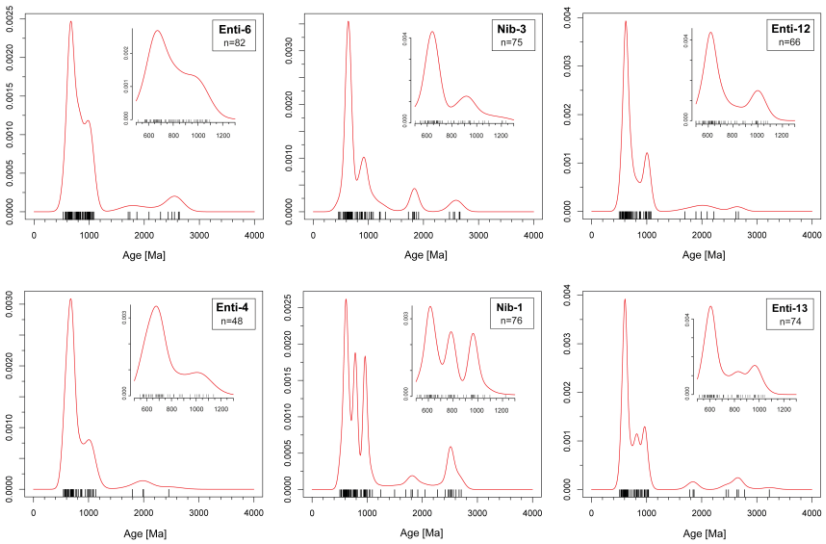
Enti-6
n=82
Nib-3
n=75
Enti-12
n=66
Enti-4
n=48
Nib-1
n=76
Enti-13
n=74
Age [Ma]

Figure 4

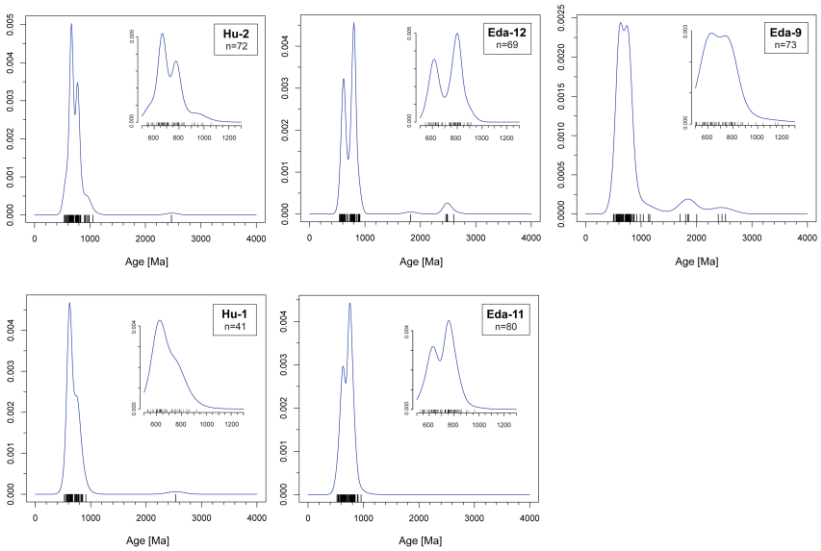

Figure 5

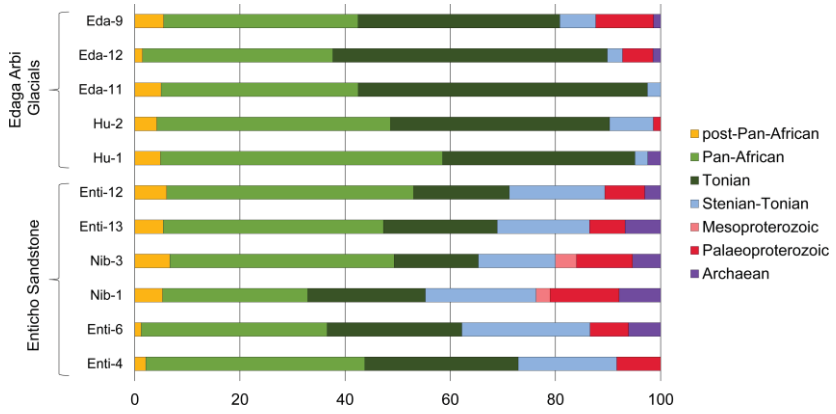
Edaga Arbi Glacials
Eda-9
Eda-12
Eda-11
Hu-2
Hu-1
Enticho Sandstone
Enti-12
Enti-13
Nib-3
Nib-1
Enti-6
Enti-4
0
20
40
60
80
100
post-Pan-African
Pan-African
Tonian
Stenian-Tonian
Mesoproterozoic
Palaeoproterozoic
Archaean

Figure 6

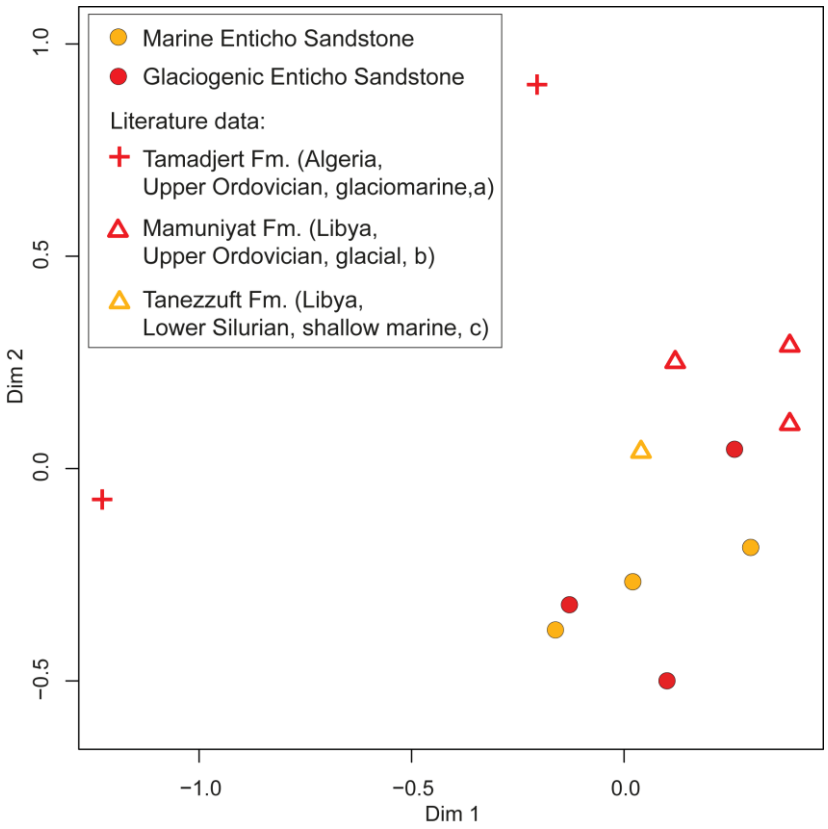
Marine Enticho Sandstone
Glaciogenic Enticho Sandstone
Literature data:
Tamadjert Fm. (Algeria,
Upper Ordovician, glaciomarine,a)
Mamuniyat Fm. (Libya,
Upper Ordovician, glacial, b)
Tanezzuft Fm. (Libya,
Lower Silurian, shallow marine, c)
Dim 2
1.0
0.5
0.0
−0.5
−1.0
−0.5
0.0
Dim 1

Figure 7

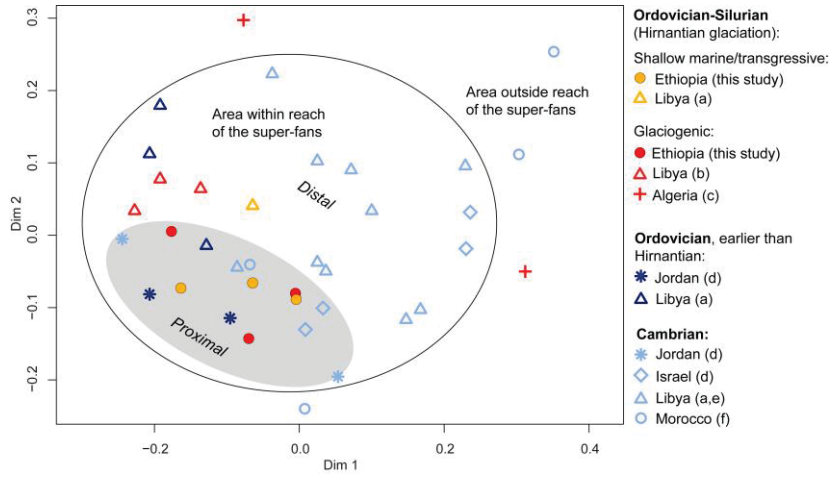
Area within reach
of the super-fans
Area outside reach
of the super-fans
Distal
Proximal
Dim 1
Dim 2
−0.2
0.0
0.2
0.4
−0.2
−0.1
0.0
0.1
0.2
0.3
Ordovician-Silurian
(Hirnantian glaciation):
Shallow marine/transgressive:
Ethiopia (this study)
Libya (a)
Glaciogenic:
Ethiopia (this study)
Libya (b)
Algeria (c)
Ordovician, earlier than
Hirnantian:
Jordan (d)
Libya (a)
Cambrian:
Jordan (d)
Israel (d)
Libya (a,e)
Morocco (f)

Figure 8

Table 1

Sample	Latitude (°)	Longitude (°)	Formation	Strati-graphic assignment	Lithology	Ages deter-mined	Concor-dant ages	% concor-dant ages
Enti-4	039.71262	13.83465	Enticho	U	Diamictite	54	48	89
Enti-6	039.74827	13.88842	Enticho	B	Sandstone	85	82	96
Enti-12	039.42093	14.49627	Enticho	LF	Sandstone	85	66	78
Enti-13	039.41911	14.49275	Enticho	LF	Sandstone	86	74	86
Nib-1	039.48972	14.25194	Enticho	B	Sandstone	85	76	89
Nib-3	039.49583	14.25222	Enticho	B	Sandstone	86	75	87
Eda-9	039.32235	13.90915	Edaga Arbi	B	Sandstone	89	73	82
Eda-11	039.00042	13.61842	Edaga Arbi	LF	Sandstone	85	80	94
Eda-12	039.19745	13.17844	Edaga Arbi	B	Sandstone	73	69	95
Hu-1	037.05068	10.31057	Edaga Arbi	LF	Sandstone	47	41	87
Hu-2	037.05068	10.31057	Edaga Arbi	LF	Sandstone	77	72	94